J Solid State Electrochem (2007) 11:1355–1364
DOI 10.1007/s10008-007-0307-3

REVIEW

Ruthenium-based electrocatalysts for oxygen reduction reaction—a review

Jong-Won Lee · Branko N. Popov

Received: 5 January 2007 / Revised: 19 January 2007 / Accepted: 14 March 2007 / Published online: 21 April 2007

Abstract A major impediment to the commercialization of fuel cells is the low activity of electrocatalysts for the oxygen reduction reaction that involves multiple electron transfer steps. Platinum is considered the best cathode catalyst toward oxygen reduction to water; however, Pt remains an expensive metal of low abundance, and it is of great importance to find Pt-free metal alternatives. Among various Pt-free catalysts under development, ruthenium-based compounds show significant catalytic activity and selectivity for four-electron reduction of oxygen to water in acidic environments. This article provides a short review on the different classes of Ru-based catalysts focusing on the catalytically active reaction sites and the oxygen reduction mechanism in acidic media. After a brief discussion of the oxygen reduction kinetics on a pure Ru metal, the paper reviews the catalytic properties of the selected Ru compounds, including crystalline Chevrel-phase chalcogenides, nanostructured Ru and Ru–Se clusters, and Ru–N chelate compounds.

Keywords Ruthenium · Electrocatalyst · Oxygen reduction · Low-temperature fuel cell

Introduction

Platinum is considered the best cathode catalyst for low-temperature fuel cells such as proton exchange membrane fuel cell and direct methanol fuel cell (DMFC), as it provides the lowest overpotential and the highest selectivity toward direct oxygen reduction to water (i.e., small amount of hydrogen peroxide [H_2O_2]) [1–4]. Even on pure Pt, however, potentials in excess of 0.3 V are lost from the thermodynamic potential for oxygen reduction because of competing water activation reaction and sluggish kinetics. Furthermore, oxygen undergoes nondissociative adsorption on Pt metals accompanied by some dissociative adsorption, which results in Pt oxidation. Most importantly, Pt remains an expensive metal of low abundance.

Two technological approaches are underway for Pt loading reduction in membrane-electrode assembly (MEA) to reduce the overall cost of fuel cells. One approach is to make use of binary or ternary Pt-transition metal alloy catalysts in MEA. It is known [4, 5] that alloying Pt with Fe, Co or Ni can increase the oxygen reduction activity so it can lower the total Pt loading in MEA. The reasons for the higher catalytic activity of Pt alloys are as follows: (1) the increase in the resistance to particle sintering, (2) surface roughening because of the removal of some alloying metal, (3) preferential crystallographic orientation, and (4) a more favorable Pt–Pt interatomic distance. However, it has frequently been reported [4, 6, 7] that a considerable amount of transition metal leaches out of the alloy catalysts under fuel cell operating conditions, causing a loss of the catalytic activity. The dissolved transition metal ions

This paper is dedicated to Professor Su-Il Pyun, who has pioneered advances in interfacial electrochemistry in the field of corrosion and materials science in South Korea, on the occasion of his 65th birthday.

J.-W. Lee (✉) · B. N. Popov
Department of Chemical Engineering,
Center for Electrochemical Engineering,
University of South Carolina,
Columbia, SC 29208, USA
e-mail: leejong@engr.sc.edu

replace the protonic sites attached to the sulfonic acid groups in the ionomer, which results in a decrease in the proton conductivity of the membrane.

The other approach is to develop Pt-free metal catalysts based on transition metals, Pd or Ru. Since of Jasinski's [8] discovery of the catalytic properties of cobalt-phthalocyanines, there has been a considerable research on non-precious metal catalysts such as: (1) porphyrin-based macrocyclic compounds of transition metal (e.g., Co-phthalocyanines and Fe-tetramethoxyphenyl porphyrin) [9–22], (2) vacuum-deposited Co and Fe compounds (e.g., Co–C–N and Fe–C–N) [23, 24], and (3) metal carbides, nitrides, and oxides (e.g., FeC_x, TaO_xN_y, MnO_x) [25, 26]. However, the above catalysts are unlikely to meet the requirements of cathode catalysts because of the far lower oxygen reduction activity in comparison to the state-of-the-art Pt-based catalysts. They show a low catalytic selectivity toward the four-electron reduction in oxygen to water, producing a large amount of H_2O_2 (typically higher than 10%), and exhibit very low electrochemical stability in acidic environments. In the case of metal-nitrogen chelate catalysts, H_2O_2 is responsible for the deterioration of electrode performance over time, as it destroys the active reaction sites by the oxidation of nitrogen ligands and hence accelerates the dissolution of transition metals [15, 27]. In addition, the polymer electrolyte membrane degrades over time because of the attack by peroxide radicals [13].

Another class of Pt-free catalysts that has attracted the most attention over the years is the Ru-based compound that contains chalcogen elements, mostly selenium [28–49]. Ru-based chalcogenide compounds, e.g., $Mo_4Ru_2Se_8$ and Ru_xSe_y, show more promising catalytic properties as compared with Pt-free catalysts based on transition metal macrocyclic complexes. Further, a recent study on chalcogen-free RuN_x chelate compounds [50, 51] has demonstrated comparable catalytic activity and selectivity to Pt-based catalysts for four-electron oxygen reduction in acidic media. Ru-based catalysts are also considered the promising alternative to Pt for cathode catalysts in DMFCs, owing to their high tolerance to methanol (CH_3OH) oxidation [32, 36, 46, 52, 53]. Unlike Pt, the Ru-based catalyst is hardly depolarized in the presence of methanol because there are no available surface sites for methanol adsorption because of the strongly adsorbed oxygenated species [36].

This article reviews the different types of Ru-based catalysts under development, focusing on the catalytically active reaction sites and the oxygen reduction mechanism in acidic media. After a brief introduction of the oxygen reduction kinetics on a pure Ru metal, the paper provides a review on the catalytic properties of the selected Ru compounds as follows: (1) crystalline Chevrel-phase chalcogenides, (2) nanostructured Ru and Ru_xSe_y clusters, and (3) RuN_x chelate compounds.

Oxygen reduction reaction on Ru metal electrode in acidic media

Although extensive experimental work has been performed to study the electrochemical behavior of a pure Ru metal electrode in both acidic and alkaline electrolytes [54–57], the mechanism of oxygen reduction is still not clearly understood for the following reasons: the surface oxidation of a Ru metal electrode starts to occur in a low potential range below 0.25 V(NHE) even before hydrogen desorption is completed, which makes a clear distinction between the two reactions very difficult. Furthermore, the oxidation state, structure, and thickness of surface oxides significantly vary with potential and time during electrochemical experiments.

Basic information regarding the catalytic properties of a Ru metal electrode in acidic electrolyte can be obtained from a research paper by Anastasijević et al. [54]. Figure 1 shows polarization curves for oxygen reduction on the rotating Ru disk electrode as a function of rotation rate [54]. The rotating disk electrode (RDE) experiments were conducted in 0.1 M $HClO_4$ saturated with oxygen by using a potential scan rate of 50 mV s^{-1}. The RDE data show that the Ru metal electrode exhibits an onset potential for oxygen reduction as high as 0.4 V(SCE), and the oxygen reduction reaction proceeds under the mixed kinetic and diffusion control. However, a diffusion limiting current is not clearly observed in the polarization curves even below −0.2 V(SCE).

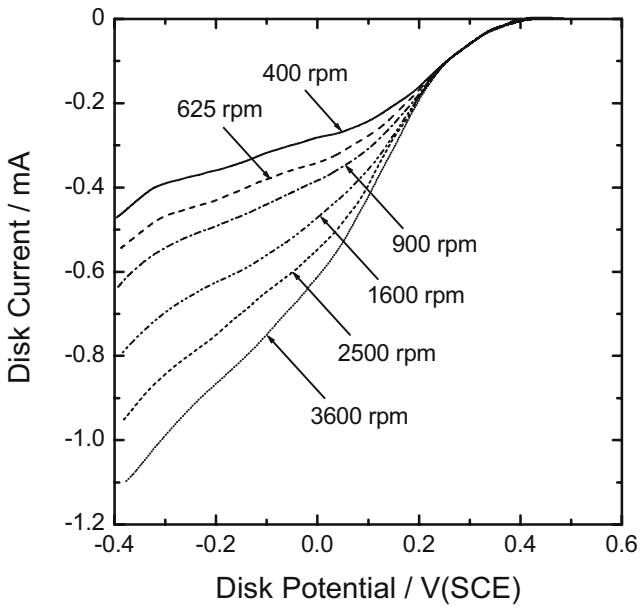

Fig. 1 Polarization curves for oxygen reduction on the rotating Ru disk electrode as a function of rotation rate. The experiments were conducted in 0.1 M $HClO_4$ saturated with oxygen by using a potential scan rate of 50 mV s^{-1}. Reproduced from [54] with permission from Elsevier

In general, the oxygen reduction reaction proceeds by two parallel pathways as follows [58]:

$$\begin{array}{ccccc} & & \overset{k_1}{\longleftarrow} & & \\ & & \uparrow \quad \downarrow & & \\ O_{2,b} & \rightarrow O_{2,a} & \xrightarrow{k_2} H_2O_{2,a} & \xrightarrow{k_3} H_2O & \\ & & \downarrow k_4 & & \\ & & H_2O_{2,b} & & \end{array} \quad (1)$$

where subscripts a and b denote the species adsorbed on the electrode surface and that in the bulk, respectively. O_2 may be directly reduced to H_2O through four-electron transfer (path 1). In parallel, O_2 may be reduced to H_2O through a series pathway involving the formation of H_2O_2 intermediate species (path 2) and the electrochemical decomposition of H_2O_2 to H_2O (path 3).

On the basis of the above reaction scheme, Anastasijević et al. [54] determined quantitatively the relevant kinetic rate constants k_1, k_2, and k_3 for oxygen reduction on the Ru metal electrode from the rotating ring disk electrode (RRDE) data. It was assumed that the rate constant k_4 for transport of the adsorbed H_2O_2 to the bulk electrolyte is negligibly small ($k_4 \approx 0$) in the potential range under the study. The analysis showed the increase of the rate constant in the order of k_1, k_3, and k_2 in the potential range between 0 and 0.13 V(SCE), which indicates that O_2 is reduced to H_2O predominantly via a series pathway (paths 2 and 3). Therefore, one can expect the catalytic selectivity of the Ru metal electrode toward complete oxygen reduction to water to be determined by the kinetics of H_2O_2 reduction.

The polarization experiments for H_2O_2 reduction in 0.1 M $HClO_4$ solution containing 3.8×10^{-6} M H_2O_2 indicated that the catalytic activity of a Ru metal for H_2O_2 reduction to H_2O gradually decreases with increasing positive potential limit [54]. The ellipsometric studies of Velikodnyi et al. [59] demonstrated that in acidic media, the Ru metal surface is covered by RuO_x with $0<x<1$ in the potential range between 0 and 0.7 V(NHE), and RuO_x with $1<x<2$ is formed when the potential is increased beyond 0.7 V(NHE). It is thus inferred that the higher the oxidation degree of the Ru metal surface is, the lower is the catalytic activity for H_2O_2 decomposition. It follows that the oxidation degree of the Ru metal surface would determine the catalytic selectivity for complete oxygen reduction to water. Actually, the Ru metal electrode is known to predominantly catalyze oxygen reduction to H_2O_2 rather than to H_2O [38], which is due to the presence of Ru surface oxides with lower activity for H_2O_2 decomposition to H_2O.

Ru-containing chalcogenides of the Chevrel-phase type

Transition metal chalcogenide compounds known as the "Chevrel phases" [60], i.e., M_6X_8 (M=high valent transition metal and X=S, Se, Te), have initially attracted the attention of solid-state chemists and physicists because of remarkable high-temperature and high-field superconducting properties [61]. Alonso-Vante et al. [28] were the first to report that Ru-containing chalcogenides of the Chevrel-phase type (e.g., $Mo_4Ru_2Se_8$) show a significant catalytic activity for oxygen reduction in acidic media.

As an example, Fig. 2 displays the currents measured on the $Mo_{4.2}Ru_{1.8}Se_8$ disk and the Pt ring as a function of disk potential [29]. The RRDE experiments were performed in 0.5 M H_2SO_4 saturated with oxygen by using a disk potential scan rate of 5 mV s^{-1}. The ring potential was held at 1.44 V(NHE) to oxidize H_2O_2 generated during the oxygen reduction reaction. The dashed line in Fig. 2 represents the background double-layer charging current measured in a deaerated solution under the same experimental conditions. It is seen in Fig. 2 that the $Mo_{4.2}Ru_{1.8}Se_8$

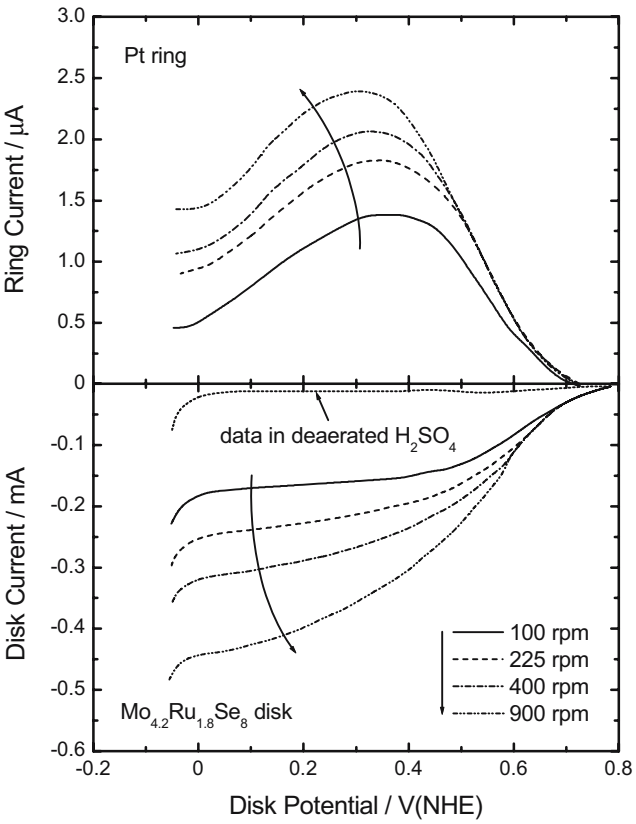

Fig. 2 Currents measured on the $Mo_{4.2}Ru_{1.8}Se_8$ disk and the Pt ring as a function of disk potential. The RRDE measurements were performed in 0.5 M H_2SO_4 saturated with oxygen by using a disk potential scan rate of 5 mV s^{-1}. The ring potential was held at 1.44 V (NHE). The data measured in a nitrogen-saturated solution were also presented. Reproduced from [29] with permission from the Journal of the American Chemical Society

catalyst exhibits an onset potential for oxygen reduction of ca. 0.8 V(NHE). The ring current increases with decreasing disk potential, then reaches a maximum value between 0.4 and 0.3 V(NHE), and finally decreases with further decreasing disk potential. The percentage of H_2O_2 produced was calculated from Fig. 2 using the well-known equation [62]:

$$\%\ H_2O_2 = \frac{200(I_r/N)}{I_d + (I_r/N)} \quad (2)$$

where I_d, I_r, and N mean the disk current, the ring current, and the collection efficiency, respectively. The value of N was taken as 0.31 in [29]. The calculation showed that the $Mo_{4.2}Ru_{1.8}Se_8$ catalyst generates only 2.8–3.9% H_2O_2 during oxygen reduction over the whole potential range, which indicates that oxygen is predominantly reduced to water via four-electron transfer. Such a high selectivity for four-electron oxygen reduction to water is quite remarkable, because a Ru metal electrode mainly catalyzes two-electron oxygen reduction to H_2O_2 as discussed in the preceding section.

Figure 3a illustrates the schematic diagram of the fundamental structural unit of a Chevrel phase (Mo, $Ru)_6Se_8$. In a Chevrel phase structure, an octahedral cluster with six metal atoms is encased in a cube of chalcogens. The mean interatomic distances between metals and between metal and selenium are ca. 0.268–0.270 nm and ca. 0.260 nm, respectively, depending on the stoichiometry of mixed metal cluster. It is well known [29, 63] that (Mo, $Ru)_6Se_8$ exhibits semiconducting properties with an energy gap between valence and conduction bands of ca. 1.3 eV. The valence band structure of $Mo_4Ru_2Se_8$ determined by X-ray photoelectron spectroscopy (XPS) is presented in Fig. 3b [36]. Note that the energy scale is referred to the Fermi level E_F. The metal–metal interactions in the octahedral cluster lead to a high density of *d*-states near the top of the valence band. In particular, Ru atoms in the cluster make the compound a "degenerate" *p*-type semiconductor, namely, E_F is located just near the top of the valence band, as shown in Fig. 3b [29, 37]. Consequently, the octahedral mixed metal clusters of Mo and Ru with a high density of *d*-states serve as the electron reservoirs where the adsorbed oxygen molecule can directly exchange electrons with the catalyst upon cathodic polarization, resulting in high catalytic activity and selectivity.

Nanostructured Ru and Ru_xSe_y clusters

Besides the fact that Ru-based chalcogenides of the Chevrel-phase type show high catalytic activity and selectivity for oxygen reduction, they are typically synthesized by a solid-state reaction of pure elements at elevated temperatures (1,200 to 1,700 °C) and pressures (0.7 GPa) [29, 48], which makes the synthesis procedure very complicated and costly. To circumvent those problems, low-temperature methodologies have been developed by different researchers to prepare Ru or Ru chalcogenide clusters. The synthesis methods are divided broadly into two categories as follows: (1) thermolysis of triruthenium dodecacarbonyl ($Ru_3(CO)_{12}$) [30, 31, 37–41, 44, 46] and (2) colloid method involving chemical reduction of ruthenium trichloride ($RuCl_3$) [37, 47].

The former method involves the thermochemical reaction of $Ru_3(CO)_{12}$ and/or elemental selenium in either xylene ($C_6H_4(CH_3)_2$) or 1,2 dichlorobenzene ($C_6H_4Cl_2$) solvent. The reaction proceeds under refluxing conditions at the boiling point of the solvent in an inert atmosphere. The compound synthesized by thermolysis of carbonyl precursors is sometimes called "carbonyl-tailored" catalyst in literature [64]. Alternatively, Ru_xSe_y catalysts can be prepared through the thermochemical treatment of colloidal Ru particles in Se-saturated xylene solvent under refluxing conditions. In the latter colloid method, a precursor $RuCl_3$ dissolved in tetrahydrofuran (THF, C_4H_8O) is chemically

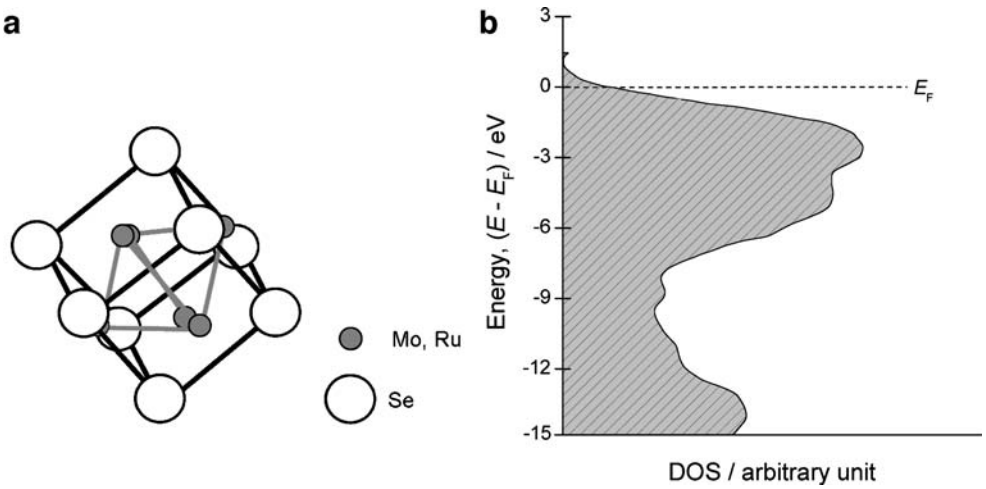

Fig. 3 **a** Schematic diagram of a Chevrel phase $(Mo,Ru)_6Se_8$ structure, and **b** density of states (*DOS*) curves for the valence band in $Mo_4Ru_2Se_8$ determined by XPS. In **b**, the energy scale is referred to the Fermi level E_F. Reproduced from [36] with permission from Elsevier

reduced by $N(C_8H_{17})_4BEt_3H$ in the presence of ethanol, resulting in nanosized Ru clusters. For the preparation of Ru_xSe_y catalysts, the synthesized colloidal Ru particles are further treated with an aqueous selenious acid (H_2SeO_3). In addition, a new process was recently developed to synthesize Ru_xSe_y catalysts supported on porous carbon on the basis of the impregnation and reduction of Ru salts [65, 66]. For instance, porous carbon powders are impregnated with a mixture of $RuCl_3$ and THF under stirring conditions, and then $RuCl_3$ is reduced on the carbon support by $LiBet_3H$/THF. Finally, Ru_x/C powder specimen is treated with H_2SeO_3 to produce Ru_xSe_y/C catalysts [65].

Tributsch et al. [37] carried out an in-depth structural analysis to identify catalytic reaction sites for oxygen reduction on the carbonyl-tailored Ru_xSe_y catalysts. X-ray diffraction (XRD) and transmission electron microscopy (TEM) studies revealed that nanosized Ru particles with a diameter of ca. 4 nm are covered with thin amorphous layers that contain carbon and oxygen species in addition to Ru and Se. Further, thermogravimetric experiment combined with mass spectroscopy showed that the ionized species CO^+ and CO_2^+ were released from the catalyst particles upon heat-treatment above 90 °C. This indicates that the surface of Ru_xSe_y catalyst is modified by carbon species, most probably carbonyl groups.

Based on the experimental findings of material characterization studies, the authors have proposed a structure of catalytic reaction sites on the carbonyl-tailored Ru_xSe_y catalyst that is schematically illustrated in Fig. 4. In Fig. 4, Ru atoms form an octahedral cluster to which carbonyl groups are attached, and a carbon atom resides in the center of octahedral Ru cluster. Such a Ru/carbido/carbonyl complex formed on a metallic Ru nanoparticle serves as the catalytic reaction site for oxygen reduction. It was also suggested that carbonyl ligands in the complex not only stabilize the interfacial Ru atoms, thus keeping them from being oxidized, but also modify the distribution of interfacial electronic states in such a way as to facilitate cathodic electron transfer.

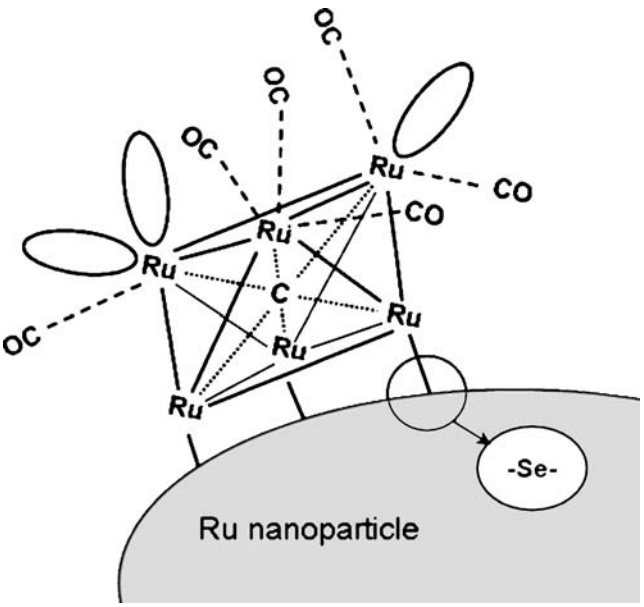

Fig. 4 Schematic diagram of active reaction sites for oxygen reduction on the carbonyl-tailored Ru_xSe_y catalyst proposed by Tributsch et al. [37]

Figure 5 presents the plot of kinetic current density i_k for oxygen reduction versus Se content in the carbonyl-tailored Ru_xSe_y catalyst obtained by Bron et al. [38]. Here, i_k means the oxygen reduction current density determined in the absence of diffusion limitations, and it was measured at 0.6 V(NHE) in 0.5 M H_2SO_4 saturated with oxygen in Ref. [38]. The i_k value continues to increase with rising Se content until it reaches a maximum at 15 mol%, indicating the positive effect of Se on the catalytic activity toward oxygen reduction. In addition, Fig. 6 envisages the percentages of H_2O_2 produced on the Ru_xSe_y catalysts with different Se contents [38]. It is seen that the catalyst containing 14.3 mol% Se generates ca. 7% H_2O_2 at 0.7 V(NHE) in comparison to ca. 22% for the Se-free Ru cluster during oxygen reduction, that is, Se improves the catalytic selectivity toward four-electron reduction of oxygen to water.

There has been much debate regarding the beneficial effect of Se on the catalytic properties of the Ru_xSe_y catalyst. The model of Tributsch et al. [37] in Fig. 6 assumes that Se facilitates the catalytic reaction by acting as a bridge to transfer electrons between the Ru/carbido/

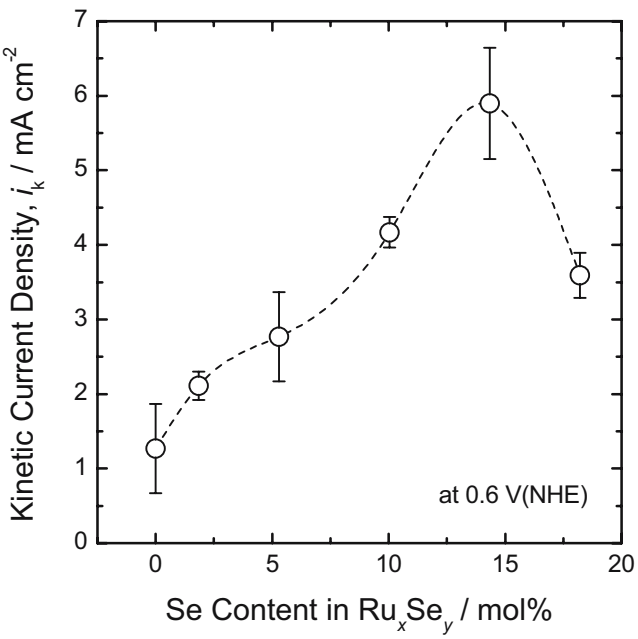

Fig. 5 Plot of kinetic current density i_k versus Se content in the carbonyl-tailored Ru_xSe_y catalyst. The values of i_k were determined at 0.6 V(NHE) in 0.5 M H_2SO_4 saturated with oxygen. Reproduced from [38] with permission from Elsevier

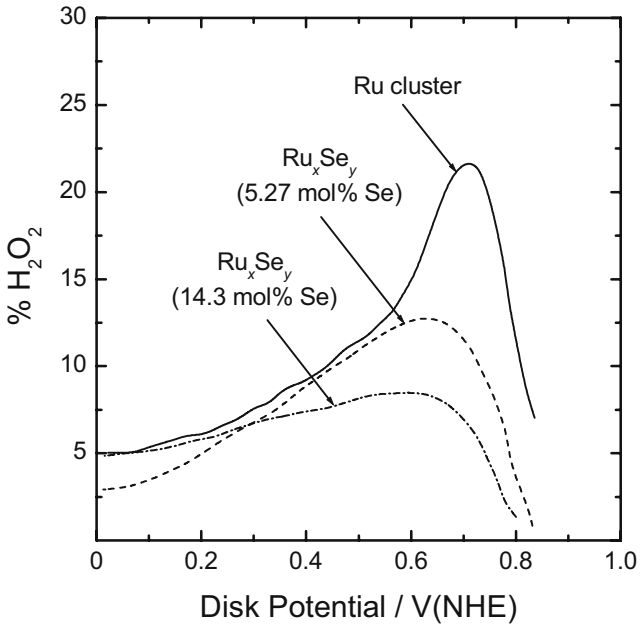

Fig. 6 Percentages of H_2O_2 produced during oxygen reduction on the carbonyl-tailored Ru_xSe_y catalysts with different Se contents as a function of disk potential. Reproduced from [38] with permission from Elsevier

carbonyl complex and the colloidal Ru nanoparticle. On the other hand, Bron et al. [38] observed that the Tafel slope obtained from the polarization curves for oxygen reduction decreased from 146.2 to 96.6 mV dec^{-1} with increasing Se content from 0 to 14.3 mol% and claimed that the Tafel slope change could be observed only when Se directly modifies the structure of the Ru/carbido/carbonyl complex. From the analysis of the infrared spectra, the authors found that such intermediate complexes as $Ru_6C(CO)_{17}$ and $Ru_6C(CO)_{14}(C_6H_4Me_2)$ are formed during catalyst preparation and that a higher Se content results in a lower amount of intermediate complexes in the precursor solution taken after the completion of thermolysis. This result suggests that Se further reacts with intermediate complexes, producing the Se-containing Ru/carbido/carbonyl complex. It was concluded that Se replaces carbonyl groups via ligand exchange reaction thus resulting in the formation of catalyst particles with an Se-modified ligand shell that are favorable for oxygen reduction.

Bron et al. [38] also speculated that the surface modification of the catalyst by Se increases the resistance to electrochemical oxidation of interfacial Ru atoms. This hypothesis is strongly supported by a recent experimental study by Schulenburg et al. [47]. Figure 7 presents the plots of anodic charge versus logarithmic time measured for the carbon-supported Ru and Ru_xSe_y catalysts prepared by colloid method [47]. The potential step experiments were conducted in 0.5 M H_2SO_4 that was deaerated by bubbling with nitrogen, and the potential was shifted from 0.05 V (NHE) to different values of 0.4–0.8 V(NHE). Under this condition, electrochemical oxidation of Ru surface is primarily responsible for the measured anodic charge. As shown in Fig. 7, the anodic charge was determined to be much lower for the Ru_xSe_y/C catalyst as compared with the Ru/C catalyst over the whole potential and time ranges, which indicates that the Ru_xSe_y/C catalyst is more resistant to electrochemical oxidation than the Ru/C catalyst. The authors proposed that Se in the Ru_xSe_y cluster occupies electrocrystallization sites for RuO_x formation thereby increasing the oxidation resistance. Keeping in mind that the catalytic properties of Ru-based catalysts are significantly affected by the oxidation degree of Ru surface oxides, it is obvious that the increased oxidation resistance of Se-containing Ru catalysts contributes to the enhanced activity and selectivity.

In a recent review paper, Alonso-Vante [64] provided a quite different perspective on catalytic reaction sites on the electrocatalysts prepared by thermolysis of $Ru_3(CO)_{12}$ precursor as follows:

$$Ru_3(CO)_{12}+ySe \rightarrow \left[Ru_xSe_y-CO_z\right] \rightarrow Ru_xSe_y+zCO \quad (3)$$

During preparation of Ru–Se catalysts, a polynuclear chemical precursor in the form of $[Ru_xSe_y–CO_z]$ is produced in the first stage. As a matter of fact, the formation of $Ru_4Se_2(CO)_{11}$ was confirmed by ^{13}C nuclear magnetic resonance analysis [64]. The author claimed that the complete loss of carbonyl groups is necessarily achieved

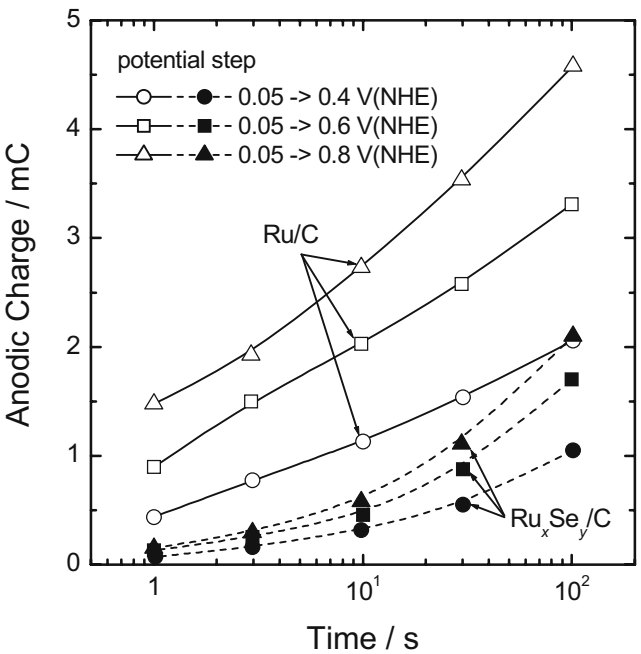

Fig. 7 Plots of anodic charge versus logarithmic time measured for the Ru/C and Ru_xSe_y/C catalysts prepared by a colloid method. The experiments were performed by shifting the potential from 0.05 V (NHE) to different values in 0.5 M H_2SO_4, which was deaerated by bubbling with nitrogen. Reproduced from [47] with permission from Elsevier

when the precursor solution is refluxed for 20 h, and the polynuclear chemical precursors are transformed into a cluster-like Ru_xSe_y material with no carbonyl ligands. This mechanism does not support the conclusion that the Ru/carbido/carbonyl complex on metallic Ru nanoparticles are catalytically active for oxygen reduction. Instead, Se atoms occupy the surface sites of Ru cluster randomly.

Using TEM, XPS, and extended X-ray absorption fine structures (EXAFS), Zaikovskii et al. [65] have provided a detailed structural analysis of the Ru_xSe_y/C catalyst prepared by the impregnation/reduction method. They have shown that for the low Se content (y/x <0.59) in Ru_xSe_y catalyst, small Ru selenide clusters (<1 nm) are formed on the surface of Ru particles; whereas for the high Se content ($y/x \approx 1.0$), core-shell structures are formed comprising hexagonally packed Ru cores and Ru selenide shells with lamellar structure. According to this view, Se atoms occupying the Ru cluster surface sites may change the electronic nature of the cluster: favorable electronic states for oxygen reduction are formed between Se 4*p* and Ru 4*d* orbitals in the molecular cluster [67]. Furthermore, an increased oxidation resistance of Ru_xSe_y catalyst could be attributed to the presence of Se atoms coordinated at the surface of Ru clusters protecting them from electrochemical oxidation.

RuN_x chelate electrocatalysts

A new class of Ru-based electrocatalyst, RuN_x, was recently developed by Liu et al. [51] using the nitrogen-chelation method. In this approach, ruthenium trichloride ($RuCl_3$) and propylenediamine ($CH_3CH(NH_2)CH_2NH_2$) were used as the Ru- and N-precursors, respectively. A mixture of $RuCl_3$ and isopropyl alcohol is refluxed at 80–90 °C under stirring conditions. Then propylenediamine is added into the solution, followed by the addition of carbon black powders under refluxing conditions, to form Ru–N complexes on the carbon support. The resulting powder specimens are heat-treated in an inert atmosphere at high temperatures ranging from 600 to 900 °C.

High-temperature pyrolysis has a critical role in the formation of catalytic reaction sites for oxygen reduction. The RRDE experiments in 0.5 M H_2SO_4 saturated with oxygen showed that the as-refluxed RuN_x catalyst, which was not subjected to pyrolysis, hardly catalyzes oxygen reduction, indicating no formation of catalytic reaction sites. On the other hand, the as-pyrolized catalyst at 700 °C exhibited an onset potential for oxygen reduction as high as 0.9 V(NHE) and a well-defined limiting current below 0.6 V(NHE).

Figure 8a,b presents the XPS spectra of N 1s region for the as-refluxed and the as-pyrolized RuN_x/C catalysts, respectively [51]. The XPS spectrum of the as-refluxed catalyst exhibits a broad peak around 399.8 eV, which corresponds to the nitrogen of the ternary amine-type [68]. Upon pyrolysis, the peak splits into two broad peaks at about 398.4 and 400.4 eV, which can be assigned to the "pyridinic N" and the "pyrrolic N," respectively. The "pyridinic N" has one lone pair of electrons as well as the one electron donated to the conjugated π bond system, so it provides an orbital in the plane of the graphene layer that can coordinate the metal ions [69, 70]. It is thus reasonable that the high-temperature pyrolysis leads to the formation of Ru clusters coordinated with pyridinic N, and such Ru–N chelate sites are catalytically active for oxygen reduction. However, pyrolysis at higher temperatures than 700 °C caused Ru crystallite particles to agglomerate, resulting in a loss of the catalytic activity.

Figure 9 illustrates the disk currents measured on the RuN_x/C catalyst and the H_2O_2 percentages generated during oxygen reduction as a function of disk potential [51]. The RuN_x catalysts were prepared using different molar ratios of Ru to N in the precursor solution. The RRDE experiments were performed in 0.5 M H_2SO_4 saturated with oxygen by using a disk potential scan rate of 5 mV s^{-1}, and the ring potential was held at 1.2 V(NHE). The value of % H_2O_2 was calculated using Eq. 2 with N=0.39. The data clearly show that nitrogen incorporation enhances the catalytic activity and selectivity toward four-electron reduction of oxygen to water and further confirm that the N-coordinated Ru chelate sites are catalytically active for oxygen reduction. It is of importance to note that the RuN_x/C catalysts with the Ru to N ratios of 1:20 and 1:30 generated

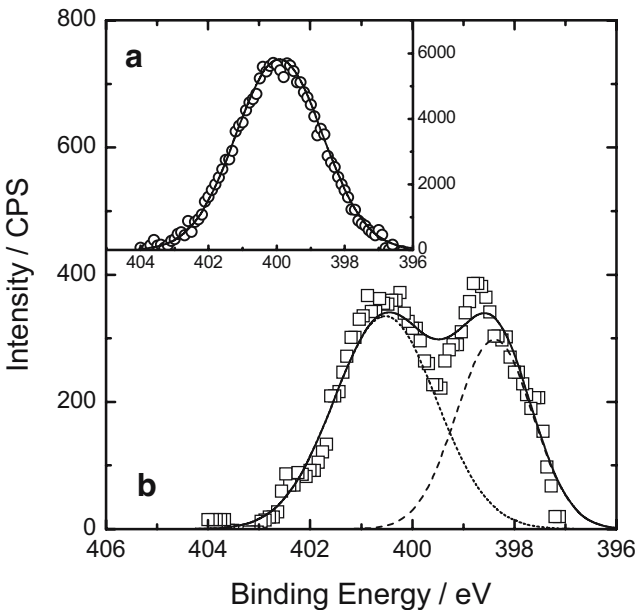

Fig. 8 XPS spectra of N 1s region for the RuN_x/C catalysts: **a** as-refluxed and **b** as-pyrolized. Reproduced from [51] with permission from the Journal of the Electrochemical Society

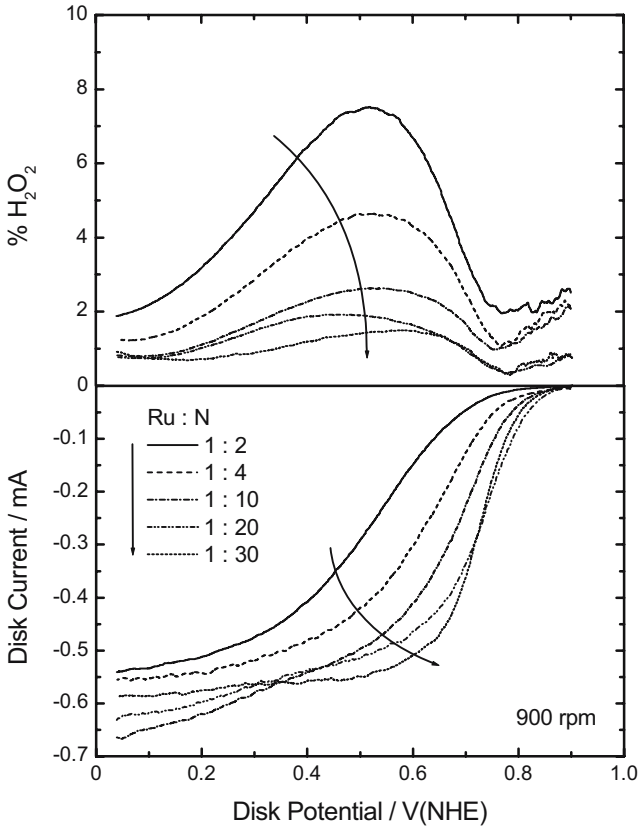

Fig. 9 Oxygen reduction currents and H_2O_2 percentages measured on the RuN_x/C catalysts prepared using different molar ratios of Ru to N in the precursor solution. The RRDE measurements were performed in 0.5 M H_2SO_4 saturated with oxygen by using a disk potential scan rate of 5 mV s^{-1}. The ring potential was held at 1.2 V(NHE). Reproduced from [51] with permission from the Journal of the Electrochemical Society

less than 2% H_2O_2 over the whole potential range, which is comparable to that for state-of-the-art Pt/C catalysts.

Bimetallic $RuMeN_x$/C catalysts with different nonnoble alloying metals (Me) were also developed using the similar chelation approach [50]. The XRD study confirmed the formation of a bimetallic alloy of hexagonal-structure with smaller lattice constants upon high-temperature pyrolysis at 800 °C. The catalytic activity for ORR increased in the order of $RuCrN_x$/C, $RuTiN_x$/C, $RuPbN_x$/C, $RuCoN_x$/C, and $RuFeN_x$/C, indicating that the nonnoble metal in the bimetallic catalyst plays a crucial role in the catalytic activity. The $RuFeN_x$/C catalyst exhibited only 30 mV higher overpotential for oxygen reduction in comparison to the conventional Pt/C catalyst.

In addition to a high catalytic activity and selectivity of RuN_x catalysts, one of the positive advantages of the chelation approach over the others is that one can easily achieve very uniform dispersion of nanosized RuN_x catalysts over porous carbon supports with high surface areas. Many attempts have been previously made to prepare the carbon-supported Ru-based chalcogenides, $(MoRu)_6Se_8$/C and Ru_xSe_y/C, using conventional colloid or thermolysis method [39, 43, 44], but one has usually observed considerable agglomeration of large catalyst particles on the carbon support (Ketjen black). Figure 10a,b presents the TEM images of the RuN_x/C and $Mo_xRu_ySe_z$/C catalysts, respectively. Here, the $Mo_xRu_ySe_z$/C catalyst was prepared through thermolysis of $Ru_3(CO)_{12}$ and Se in xylene. As shown in Fig. 10a, the RuN_x catalyst particles are uniformly dispersed over the carbon support, and the mean particle sizes were estimated to be ca. 2–4 nm, whereas $Mo_xRu_ySe_z$/C has particle sizes as large as 6–8 nm (Fig. 10b).

Concluding remarks

The catalytic properties of various Ru-based compounds ranging from the Chevrel phase $(Mo,Ru)_6Se_8$ to the nanostructured Ru_xSe_y clusters to RuN_x chelate compounds were discussed in terms of the activity and selectivity toward a four-electron oxygen reduction to water. For Ru-based compounds, a high number of *d*-states concentrated in a narrow energy region are responsible for high catalytic activity and selectivity. Selenium is a critical element controlling the catalytic properties: namely, it directly modifies the electronic structure of the catalytic reaction center and increases the resistance to electrochemical oxidation of interfacial Ru atoms in acidic environments.

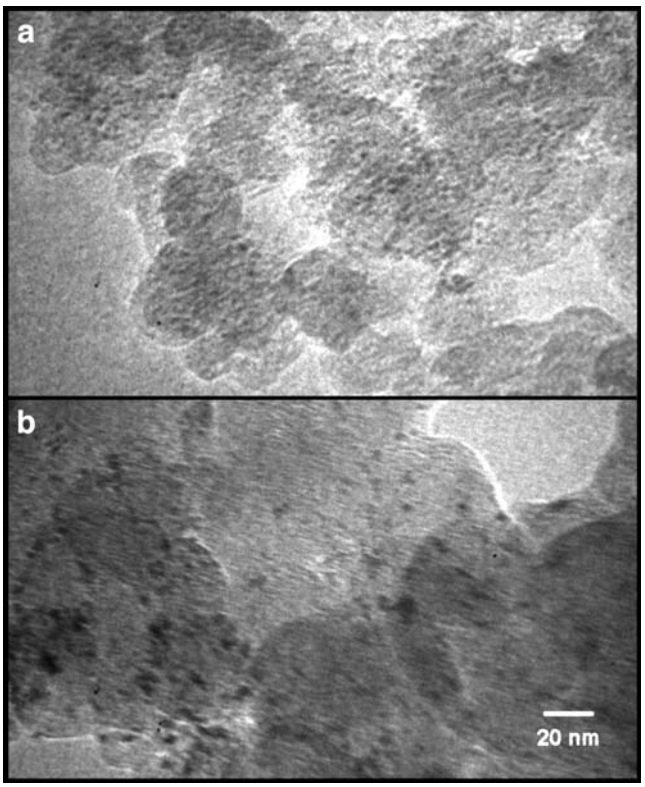

Fig. 10 TEM images of **a** RuN_x/C and **b** amorphous $Mo_xRu_ySe_z$/C

The Se-free RuN_x catalysts supported on a high-surface area carbon were recently developed, which exhibits comparable activity and selectivity to state-of-the-art Pt/C catalysts. Excellent progress is currently being made toward the optimization of MEA performance with different Ru-based cathode catalysts [42, 45, 49, 50], and substantial new literature is appearing on this technical issue.

Acknowledgment Financial support provided by the Department of Energy (DOE) is acknowledged gratefully.

References

1. Rao ML, Damjanovic BA, Bockris JOM (1963) J Chem Phys 67:2508
2. Markovic NM, Ross PN (2000) Electrochim Acta 45:4101
3. Markovic NM, Ross PN (2002) Surf Sci Rep 286:1
4. Gasteiger HA, Kocha SS, Sompalli B, Wagner FT (2005) Appl Catal B 56:9
5. Thompsett D (2003) Pt alloys as oxygen reduction catalysts. In: Vielstich W, Lamm A, Gasteiger HA (eds) Handbook of fuel cells—fundamentals technology and applications, vol 3. Wiley, Chichester, pp 467–480
6. Colón-Mercado HR, Kim H, Popov BN (2004) Electrochem Commun 6:795
7. Colón-Mercado HR, Popov BN (2006) J Power Sources 155:253
8. Jasinski R (1964) Nature 201:1212
9. Widelov A, Larsson R (1992) Electrochim Acta 37:187
10. Lalander G, Cote R, Guay D, Dodelet JP, Weng LT, Bertrand P (1997) Electrochim Acta 42:1379
11. Cote R, Lalande G, Guay D, Dodelet JP (1998) J Electrochem Soc 145:2411
12. Gouerec P, Savy M, Riga J (1998) Electrochim Acta 43:743
13. Gojkovic SLj, Gupta S, Savinell RF (1999) Electrochim Acta 45:889
14. Lefevre M, Dodelet JP, Bertrand P (2000) J Phys Chem B 104:11238
15. Schulenburg H, Stankov S, Schunemann V, Radnik J, Dorbandt I, Fiechter S, Bogdanoff P, Tributsch H (2003) J Phys Chem B 107:9034
16. Marcotte S, Villers D, Guillet N, Roue L, Dodelet JP (2004) Electrochim Acta 50:179
17. Sawai K, Suzuki N (2004) J Electrochem Soc 151:A682
18. Villers D, Jacques-Bedard X, Dodelet JP (2004) J Electrochem Soc 151:A1507
19. Sawai K, Suzuki N (2004) J Electrochem Soc 151:A2132
20. Yamazaki SI, Yamada Y, Ioroi T, Fujiwara N, Siroma Z, Yasuda K, Miyazaki Y (2005) J Electroanal Chem 576:253
21. Yuasa M, Yamaguchi A, Itsuki H, Tanaka K, Yamamoto M, Oyaizu K (2005) Chem Mater 17:4278
22. Bashyam R, Zelenay P (2006) Nature 443:63
23. Yang R, Bonakdarpour A, Easton EB, Dahn JR (2006) ECS Trans 3:221
24. Easton EB, Bonakdarpour A, Yang R, Stevens DA, O'Neill DG, Vernstrom G, O'Brien DP, Schmoeckel AK, Wood TE, Atanasoski RT, Dahn JR (2006) ECS Trans 3:241
25. Kim JH, Ishihara A, Mitsushima S, Kamiya N, Ota KI (2006) ECS Trans 3:255
26. Shimizu Y, Takase S, Otsubo T (2006) ECS Trans 3:263
27. Gupta S, Tryk D, Zecevic SK, Aldred W, Guo D, Savinell RF (1998) J Appl Electrochem 28:673
28. Alonso-Vante N, Tributsch H (1986) Nature 323:431
29. Alonso-Vante N, Jaegermann W, Tributsch H, Hönle W, Yvon K (1987) J Am Chem Soc 109:3251
30. Alonso-Vante N, Giersig M, Tributsch H (1991) J Electrochem Soc 138:639
31. Alonso-Vante N, Tributsch H, Solorza-Feria O (1995) Electrochim Acta 40:567
32. Reeve RW, Christensen PA, Hamnett A, Haydock SA, Roy SC (1998) J Electrochem Soc 145:3463
33. Solorza-Feria O, Ramírez-Raya S, Rivera-Noriega R, Ordoñez-Regil E, Fernández-Valverde SM (1997) Thin Solid Films 311:164
34. Rodríguez FJ, Sebastian PJ, Solorza O, Pérez R (1998) Int J Hydrogen Energy 23:1031
35. Alonso-Vante N, Borthen P, Fieber-Erdmann M, Strehblow HH, Holub-Krappe E (2000) Electrochim Acta 45:4227
36. Alonso-Vante N, Bogdanoff P, Tributsch H (2000) J Catal 190:240
37. Tributsch H, Bron M, Hilgendorff M, Schulenburg H, Dorbandt I, Eyert V, Bogdanoff P, Fiechter S (2001) J Appl Electrochem 31:739
38. Bron M, Bogdanoff P, Fiechter S, Dorbandt I, Hilgendorff M, Schulenburg H, Tributsch H (2001) J Electroanal Chem 500:510
39. Bron M, Bogdanoff P, Fiechter S, Hilgendorff M, Radnik J, Dorbandt I, Schulenburg H, Tributsch H (2001) J Electroanal Chem 517:85
40. Alonso-Vante N, Malakhov IV, Hikitenko SG, Savinova ER, Kochubey DI (2002) Electrochim Acta 47:3807
41. Bron M, Bogdanoff P, Fiechter S, Tributsch H (2005) J Electroanal Chem 578:339
42. Cheng H, Yuan W, Scott K (2006) Electrochim Acta 52:466
43. Kulesza, PJ, Miecznikowski K, Baranowska B, Skunik M, Fiechter S, Bogdanoff P, Dorbandt I (2006) Electrochem Commun 8:904
44. Leveratto D, Racz A, Savinova ER, Stimming U (2006) Fuel Cells 6:203
45. González-Huerta RG, Chávez-Carvayar JA, Solorza-Feria O (2006) J Power Sources 153:11
46. Sari Ozenler S, Kadirgan F (2006) J Power Sources 154:364
47. Schulenburg H, Hilgendorff M, Dorbandt I, Radnik J, Bogdanoff P, Fiechter S, Bron M, Tributsch H (2006) J Power Sources 155:47
48. Zhang L, Zhang J, Wilkinson DP, Wang H (2006) J Power Sources 156:171
49. Suárez-Alcántara K, Rodríguez-Castellanos A, Dante R, Solorza-Feria O (2006) J Power Sources 157:114
50. Liu L, Lee JW, Popov BN (2006) J Power Sources 162:1099
51. Liu L, Kim H, Lee JW, Popov BN (2007) J Electrochem Soc 154: A123
52. Schmidt TJ, Paulus UA, Gasteiger HA, Alonso-Vante N, Behm RJ (2000) J Electrochem Soc 147:2620
53. Cao D, Wieckowski A, Inukai J, Alonso-Vante N (2006) J Electrochem Soc 153:A869
54. Anastasijević NA, Dimitrijević ZM, Adžić RR (1986) Electrochim Acta 31:1125
55. Anastasijević NA, Dimitrijević ZM, Adžić RR (1986) J Electroanal Chem 139:351
56. Prakash J, Joachin H (2000) Electrochim Acta 45:2289
57. Metikoš-Huković M, Babić R, Jović F, Grubač Z (2006) Electrochim Acta 51:1157
58. Maruyama J, Inaba M, Ogumi Z (1998) J Electroanal Chem 458:175
59. Velikodnyi LN, Sheplin VA, Kasatkin ÉV (1982) Sov Electrochem 18:1134
60. Chevrel R, Sergent M, Prigent J (1971) J Solid State Chem 3:515
61. Fisher Ø (1978) Appl Phys 16:1
62. Paulus UA, Schmidt TJ, Gasteiger HA, Behm RJ (2001) J Electroanal Chem 495:134
63. Hughbanks T, Hoffmann R (1983) J Am Chem Soc 105:1150

64. Alonso-Vante N (2006) Fuel Cells 6:182
65. Zaikovskii VI, Nagabhushana KS, Kriventsov VV, Loponov KN, Cherepanova SV, Kvon RI, Bönnemann H, Kochubey DI, Savinova ER (2006) J Phys Chem 110:6881
66. Zehl G, Dorbandt I, Schmithals G, Radnik J, Wippermann K, Richter B, Bogdanoff P, Fiechter S (2006) ECS Trans 3:1261
67. Dassenoy F, Vogel W, Alonso-Vante N (2002) J Phys Chem B 106:12152
68. Gerenser LJ, Grace JM, Apai G, Thompson PM (2000) Surf Interface Anal 29:12
69. Jia YF, Xiao B, Thomas KM (2002) Langmuir 18:470
70. Maldonado S, Stevenson KJ (2005) J Phys Chem B 109:4707